Journal of Catalysis **200,** 241–249 (2001)
doi:10.1006/jcat.2001.3206, available online at http://www.idealibrary.com on IDEAL®

Zirconia-Supported Cobalt as a Catalyst for Methane Combustion

V. G. Milt, M. A. Ulla, and E. A. Lombardo[1]

Instituto de Investigaciones en Catálisis y Petroquímica, INCAPE (FIQ, UNL-CONICET), Santiago del Estero 2829, 3000 Santa Fe, Argentina

Received August 24, 2000; revised January 3, 2001; accepted February 12, 2001; published online May 15, 2001

Cobalt-supported catalysts were prepared using two different techniques: atomic layer epitaxy (ALE) and wet impregnation. Cobalt and lanthanum acetylacetonates were used and the solvents employed were either anhydrous THF or isobutyl alcohol. ZrO_2 and La_2O_3/ZrO_2 (lanthanum-doped ZrO_2) were used as supports and La_2O_3 as reference. The most active catalysts in the 770–970 K range were those in which cobalt was incorporated using the ALE technique over ZrO_2 or La_2O_3/ZrO_2. The tested solids were characterized by XRD, TPR, and XPS. The features that differentiate good from poor catalysts are the following: good cobalt dispersion, the presence of surface Co^{2+}, a low-temperature TPR peak, the absence of bulk carbonates, and the limited amount of surface carbonates. These results are discussed in terms of the current literature. © 2001 Academic Press

Key Words: **cobalt; zirconia; atomic layer epitaxy; methane combustion.**

INTRODUCTION

The main advantage of the catalytic combustion of methane over conventional thermal combustion is the drastic decrease of NO_x formation. This is due to the fact that the temperatures of the catalytic process are lower than those achieved in free radical combustion (1, 2). In turn, this impacts on the overall energy efficiency because there is no need to inject cool air into the gas stream feeding the turbine. Catalytic combustion requires formulations with high activity over long time intervals, avoiding excessive sintering and deactivation in the hot and corrosive combustion environment.

The commercial application of catalytic combustion technology is imminent thanks to the development of stable catalysts and to the introduction of new engineering approaches. In October 1998, Catalytica Inc. installed the first commercial gas turbine equipped with a catalytic burner in an electrical utility (3).

Dalla Betta (4) proposed a hybrid combustion system design, where the catalyst temperature is limited and the combustion of fuel is completed downstream of the catalyst. The catalyst is divided into several stages that operate at different temperatures. The outlet stage operates at the required temperature so that by the end of this bed, the gas temperature initiates the homogeneous combustion process in a subsequent chamber.

Thermally stable catalysts for catalytic combustion can be achieved by combining an active transition metal oxide with a second nonactive metal oxide. This is because the most active transition metal oxides for hydrocarbon oxidation, such as CuO_x, CoO_x, and FeO_x, start sintering at two-thirds to one-half of their melting temperatures, depending on the grain size (1, 2). The incorporation of a transition metal into a thermostable structure like perovskite, ABO_3, provides an interesting route to stabilize the active component (5, 6). Cobalt perovskites show good catalytic activity for the total oxidation of methane (7–9), but the surface areas are low. In order to increase the surface areas, these active oxides should be supported on high surface area solids. Mizuno *et al.* (10) produced a highly dispersed La–Co oxide on ZrO_2 which may have $LaCoO_3$ structure. They also reported the formation of additional phases when the calcination temperature was above 1120 K. Undesired solid-state reactions often take place between the active component and the support to form other stable albeit nonactive mixed oxides. Thus, adequate preparation techniques should be used in order to ensure the retention of the active components on the catalyst surface.

The atomic layer epitaxy (ALE) technique is very attractive for the preparation of supported oxide catalysts since it allows the attainment of thin films over the supports by a controlled deposition at the atomic layer level. Better control of the building-up of surface structures is achieved by the sequential introduction of the active components in saturating gas–solid reactions, which implies the use of compounds with sufficient volatility and stability under the reaction conditions. Several metal β-diketonate complexes fulfill these requirements. Careful selection and control of the reaction temperature prevents uncontrolled deposition through condensation of the reactants or their decomposition products. Due to the utilization of surface

[1] To whom correspondence should be addressed. Fax: 54-342-4536861. E-mail: nfisico@fiqus.unl.edu.ar.

0021-9517/01 $35.00

saturation by chemisorption, ALE exhibits a self-controlling feature, allowing a homogeneous distribution of the active species through the porous support (11–15). Within this context, we focused our study on the preparation of catalysts that could work in the temperature range of 770–970 K.

The ALE technique has been employed in the preparation of cobalt supported on stable matrixes with the goal of obtaining a high dispersion of the transition metal on the surface of the supports. These supported oxides were tested as catalysts for the total combustion of methane. The supports employed were ZrO_2 and La-doped ZrO_2, while La_2O_3 was used as reference. The catalysts were characterized by X-ray diffraction (XRD), temperature-programmed reduction (TPR), and X-ray photoelectron spectroscopy (XPS).

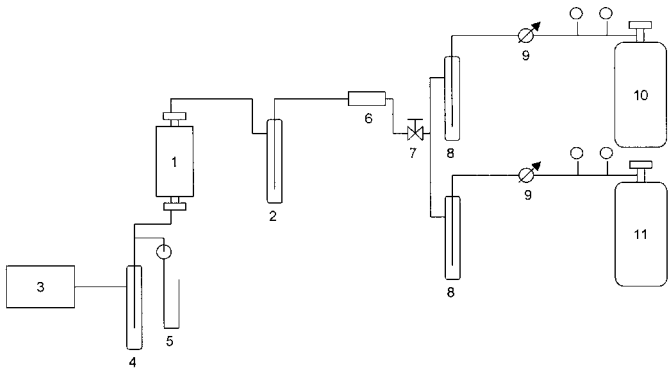

FIG. 1. Scheme of ALE apparatus: 1, reactor and oven; 2, sublimator of the organometallic compound; 3, mechanical pump; 4, solid particle trap; 5, manometer; 6, mass flow controller; 7, needle valve; 8, silica gel dryers; 9, pressure regulators; 10, N_2 cylinder; and 11, air cylinder.

EXPERIMENTAL

Catalyst Preparation

Two different supports were used: ZrO_2 (Degussa, 99,99%) and La-doped ZrO_2 (La_2O_3/ZrO_2). The ZrO_2 support was previously calcined at 870 K in air. La_2O_3/ZrO_2 was prepared by wet impregnation of ZrO_2 with a solution of lanthanum acetylacetonate ($La(acac)_3$) in anhydrous THF, evaporating the resulting suspension in an oven at 380 K for 12 h. The dry solid was calcined in air at 770 K for 4 h. The final content of lanthanum was 9.6 wt% La. Commercial La_2O_3 (Anedra, 99.99%) was used as a reference support.

Cobalt was incorporated into these supports using two different techniques: atomic layer epitaxy and wet impregnation. Cobalt(III) acetylacetonate [$Co(acac)_3$, mp 484 K] was employed with the ALE technique under the conditions summarized in Table 1. The chemisorption of the cobalt compound was carried out in a flow-type reactor operated at low pressure ($P \cong 1330$ Pa), which was designed and constructed with this purpose (Fig. 1). When cobalt was incorporated by wet impregnation, cobalt(II) acetylacetonate [$Co(acac)_2$] dissolved in isobutyl alcohol (in the proportion of 1.2 mg of $Co(acac)_2$/ml of solvent) was used. The solid was dried at 380 K for 12 h followed by calcination in air at 770 K for 4 h. All the catalysts were treated in air at 970 K for 4 h prior to being characterized and/or tested for the proposed reaction.

Table 2 shows the cobalt-supported oxides prepared. $LaCoO_3$ prepared by the explosion method (16), followed by calcination in air at 1220 K for 10 h, is included for comparison. By the nomenclature adopted, values between parentheses correspond to the cobalt weight percentage (determined by atomic absorption), a bar preceding the support indicates that the wet impregnation method was used, and where there is no bar, the ALE technique was employed, e.g., $Co(1.9)/ZrO_2$ and $Co(1.9)ZrO_2$, respectively.

Characterization

X-ray diffraction patterns were obtained with an XD-D1 Shimadzu instrument with a monochromator using Cu$K\alpha$ radiation at a scan rate of 1° min^{-1}. The BET surface area was determined by N_2 adsorption in a Quantachrome Nova 1000 Sorptometer.

TABLE 1

ALE Procedure Used in the Preparation of Co-Supported Oxides by Repeated Reaction Cycles of $Co(acac)_3$ and Calcination Sequences ($P \cong 1330$ Pa)

Preheating of the support	Sublimation and chemisorption of $Co(acac)_3$	Purge	Calcination	Purge
770 K, N_2, 1 h	440 K, N_2, 1 h	440 K, N_2, 0.5 h	770 K, air, 1 h	440 K, N_2 0.5 h
	Repeated reaction cycle			

TABLE 2

Catalysts Prepared

Catalysts[a]	Support	Preparation method	Number of ALE reaction cycles
$Co(0.42)ZrO_2$	ZrO_2	ALE	1
$Co(0.95)ZrO_2$	ZrO_2	ALE	3
$Co(1.9)ZrO_2$	ZrO_2	ALE	5
$Co(1.9)/ZrO_2$	ZrO_2	Wet impregnation	—
$Co(0.38)La/ZrO_2$	La_2O_3/ZrO_2	ALE	1
$Co(0.90)La/ZrO_2$	La_2O_3/ZrO_2	ALE	3
$Co(1.8)La/ZrO_2$	La_2O_3/ZrO_2	ALE	5
$Co(0.27)La_2O_3$	La_2O_3	ALE	3
$Co(3.3)/La_2O_3$	La_2O_3	Wet impregnation	—

[a] The numbers between parentheses indicate cobalt percentage by weight. A bar preceding the support indicates wet impregnation while no bar means that the ALE technique was used.

TPR experiments were performed using an Okhura TS-2002 instrument equipped with a thermal conductivity cell (TCD). Typically, 0.050 g of the catalyst was pretreated in oxygen at 620 K for 2 h.

The XPS spectra were obtained at room temperature with a Shimadzu ESCA 750 instrument, using Al$K\alpha$ radiation. XPS PEAK software was used to process the data. XPS intensity ratios were determined using the integrated areas of the Co $2p_{3/2}$ and La $3d_{5/2}$ photoelectron lines (including the satellite peaks), and the sum of the integrated areas of Zr $3d_{5/2}$ and Zr $3d_{3/2}$ signals, considering the overlapping of the two lines. The integrated areas were corrected taking into account the Scofield photoelectron cross sections.

Catalytic Measurements

The catalysts were tested in a packed-bed tubular quartz reactor (i.d. 8 mm) with a 2-mm-o.d. thermowell. They were placed on a fritted quartz disk and covered by quartz wool. Mass flow controllers were used to measure the gas flows. The gas mixture consisted of 3 vol% methane, 7.2 vol% oxygen, and nitrogen balance. The total gas flow varied between 50 and 800 $cm^3 \cdot min^{-1}$(STP). The products were analyzed by using an on-line gas chromatograph using a Porapak Q column and a thermal conductivity detector (TCD).

The reaction temperature range explored was 770–970 K. To evaluate the contribution of the homogeneous reaction, the reactant mixture was flowed through the quartz wool packed reactor. At 970 K there was no detectable methane conversion (the detection limit of our system is 0.2% CH_4 conversion). The carbon balance indicates that, under our experimental conditions, the methane combustion yields only carbon dioxide. Thus, the methane conversion was calculated as the ratio between carbon dioxide concentration and the sum of methane and carbon dioxide concentrations (carbon compounds) at the reactor outlet. At least three data points were obtained at each temperature and the catalysts were evaluated from the lower (770 K) to the higher (970 K) temperatures, the time on stream being around 8–10 h. To calculate the reaction rate at 770 K, a fresh catalyst was maintained at this temperature for 0.5 h and then the conversion was evaluated. The reactor was operated in a differential mode (methane conversion below 10% was always used). Reaction rates were calculated as

$$v = \frac{aX_{CH_4}F_{CH_4}}{mS}\ (\mu\text{mol}\cdot\text{s}^{-1}\cdot\text{m}^{-2}), \qquad [1]$$

where a is a unit conversion constant (μ mol · min · $cm^{-3} \cdot s^{-1}$), X_{CH4} the methane conversion, F_{CH4} the CH_4 flow (cm^3 STP · min^{-1}), m the catalyst mass (g), and S the surface area of the catalyst (m^2[BET] · g^{-1}).

RESULTS

Catalytic Activity

Gradients detection. Experimental data obtained at 770 K were processed and analyzed in order to detect the existence of both short- and long-range effect gradients in the reacting system.

(i) Detection of possible short-range gradients. According to the criteria proposed by Carberry (17) and Heck and Farrauto (18), the following values were obtained for the most unfavorable conditions:

$$\bar{\eta}\cdot\text{Da} = 1.11\times10^{-7} \ll 0.01 \qquad [2]$$

$$\bar{\beta}_{CH_4} = 0.312 \quad \text{and} \quad \bar{\beta}_{O_2} = 0.744 \quad \text{thus} \quad \bar{\beta}.\bar{\eta}.\text{Da} \ll 0.01 \qquad [3]$$

$$\Phi_{O_2} = 3.6\times10^{-6} \ll 0.1 \quad \text{and} \quad \Phi_{CH_4} = 6.1\times10^{-6} \ll 0.1 \qquad [4]$$

$$\beta_{CH_4} = 2.45\times10^{-4} \ll 1 \quad \text{and} \quad \beta_{O_2} = 1.73\times10^{-4} \ll 1. \qquad [5]$$

[2] means that there is no significant difference between the concentrations of gas reactants in the gas phase (C) and in the interphase (Cs) since $C_s/C = 1 - \bar{\eta}\cdot\text{Da}$; [3] means that there is no interphase temperature gradient since $\frac{T_s}{T} = 1 - \bar{\beta}\cdot\bar{\eta}\cdot\text{Da}$, T_s being the temperature on the surface of the catalyst particle and T the temperature in the gas phase; while [4] and [5] mean that there are neither intraphase concentration nor temperature gradients, respectively.

(ii) In order to minimize long-range effects, conversion values between 1% and 8% were used to calculate reaction rates (Table 3). In a few cases, the rates were calculated from the slope at the origin of the conversion vs residence time plots.

Considering the maximum heat released for the 8% CH_4 conversion of the reactant mixture, the maximum temperature difference between the inlet and the outlet catalyst bed is 60 K. To check the actual temperature increase, the same kinetic experiment was run twice at the same space velocity. In the first one, 0.050 g of catalysts was used while in the second, only 0.010 g was used. In this way the heat released at 770 K was modified and so was the L/D ratio (1.5–1.0). The rates obtained were almost the same (31.0 and 31.2 $\mu\text{mol}\cdot\text{s}^{-1}\cdot\text{m}^{-2}$), thus indicating the absence of long-range thermal effects.

Besides, the activation energies reported elsewhere (19) (19–23 kcal · mol^{-1}) are consistent with the absence of both mass and heat transfer effects. This means that if there existed any temperature or concentration interparticle gradient, it would not have an appreciable effect on the reaction rate.

Table 3 shows reaction rates obtained at 770 K for all the prepared catalysts by operating our reactor in a differential mode. $LaCoO_3$ and Co_3O_4 are included for comparison.

TABLE 3

Methane Combustion over Cobalt-Containing Catalysts at 770 K[a]

Catalyst	Methane[b] conversion (%)	Reaction rate (μmol s^{-1} m^{-2}) × 10^2
$Co(0.42)ZrO_2$	2.04	21
$Co(0.95)ZrO_2$	7.22	47
$Co(1.9)ZrO_2$	2.11	66
$Co(1.9)/ZrO_2$[c]	3.21	20
$Co(0.38)La/ZrO_2$	0.90	17
$Co(0.90)La/ZrO_2$	7.94	29
$Co(1.8)La/ZrO_2$	4.31	31
$Co(0.27)La_2O_3$	2.69	4.6
$Co(3.3)/La_2O_3$	3.16	5.4
$LaCoO_3$[d]	—	4.3
La_2O_3/ZrO_2	3.77	3.4
ZrO_2	0	0
La_2O_3	1.23	2.1
Co_3O_4[e]	—	486.5

[a] Reactant composition: 3 vol% CH_4, 7.2 vol% O_2, balance N_2.
[b] Conversion data used to calculate rates.
[c] This sample was prepared by the impregnation method.
[d] Reference (7). The final calcination temperature of the perovskite is 1220 K (BET surface area 6 $m^2 \cdot g^{-1}$).
[e] Data from literature extrapolated to our evaluation conditions (19).

Note that ZrO_2 is inactive at 770 K. From the activity viewpoint, the solids prepared are clearly divided into two groups: those of cobalt supported on ZrO_2 or La_2O_3/ZrO_2 by the ALE technique, and those of cobalt–lanthanum oxides, the former group being an order of magnitude more active than the latter. The behavior of $Co(1.9)/ZrO_2$ could be considered to be in the middle. From Table 3, it can also be inferred that cobalt supported on ZrO_2 is more active than cobalt supported on La_2O_3/ZrO_2 when the ALE method is used.

Figure 2 shows the catalytic behavior of cobalt supported on ZrO_2 or La_2O_3/ZrO_2 in the whole temperature range studied: 770–970 K. Note the good performance of catalysts prepared employing the epitaxial growth technique for every temperature. At 770 K $Co(1.9)ZrO_2$ appears as the best catalyst. However, at higher temperature both the $Co(1.9)ZrO_2$ and the $Co(0.95)ZrO_2$ formulations become less active than $Co(1.8)La/ZrO_2$ and $Co(0.90)La/ZrO_2$. This is symptomatic of deactivation of the former catalysts. Nevertheless, they are still more active than $Co(1.9)/ZrO_2$. Long-term experiments (150 h on stream at 970 K) indicate that $Co(1.8)La/ZrO_2$ decreases only 33% of its initial rate value after this treatment. But in the case of both $Co(1.9)ZrO_2$ and $Co(0.95)ZrO_2$, there is a sharp decrease of 78% in the same period.

X-Ray Diffraction Analysis

The characteristics of the supports are summarized in Table 4. The XRD patterns of ZrO_2 indicate the presence of both the monoclinic and the tetragonal phases whereas in the case of La_2O_3, the structures present are La_2O_3 and $La_2O_2CO_3$. For La-doped ZrO_2 the only detected phases were those present in ZrO_2 and La_2O_3. There is no formation of $La_2Zr_2O_7$ within the limits of detection of this technique.

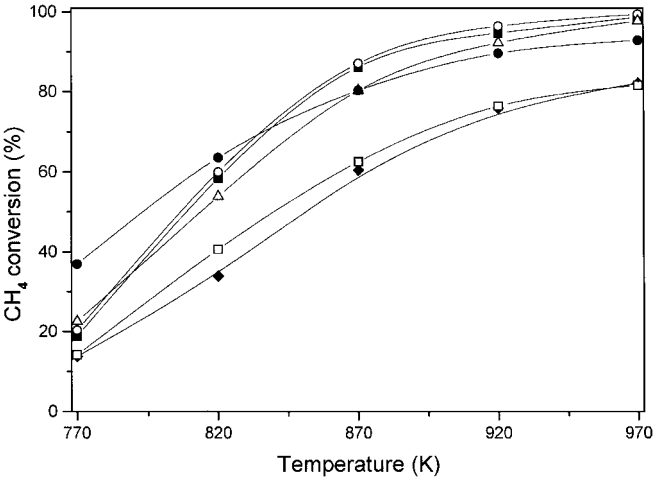

FIG. 2. Catalytic combustion of methane on ZrO_2- and La_2O_3/ZrO_2-supported cobalt: (●) $Co(1.9)ZrO_2$, (△) $Co(0.95)ZrO_2$, (□) $Co(0.42)ZrO_2$, (○) $Co(1.8)La/ZrO_2$, (■) $Co(0.90)La/ZrO_2$, and (◆) $Co(1.9)/ZrO_2$. Conditions: 3 vol% CH_4, 7.2 vol% O_2, N_2 balance, total gas flow 100 cm^3 STP · min^{-1}, catalyst mass 0.05 g.

The XRD patterns of supported cobalt over ZrO_2 or La_2O_3/ZrO_2 showed no peak that could correspond to any cobalt compound. Note that although there are solids containing about 2 wt% Co, this could not be detected by XRD (remember that all the oxides were calcined at 970 K for 4 h prior to their characterization). The diffraction pattern of $Co(0.27)La_2O_3$ shows the support signals, while $Co(3.3)/La_2O_3$ clearly exhibits the presence of $LaCoO_3$ perovskite and low-intensity Co_3O_4 reflections in addition to the support fingerprint.

BET Results

Table 4 shows the surface areas of the supports. After cobalt addition (by ALE or wet impregnation techniques),

TABLE 4

Physicochemical Features of the Supports

Support	Phases observed by XRD[a]	Surface area,[b] $m^2 \cdot g^{-1}$
ZrO_2	Monoclinic and tetragonal ZrO_2 (37-1484 and 27-997)	30
La_2O_3/ZrO_2	La_2O_3, monoclinic and tetragonal ZrO_2[c] (5-602, 37-1484, and 27-997)	30
La_2O_3	La_2O_3 and $La_2O_2CO_3$ (5-602 and 37-804)	13

[a] Values between parentheses correspond to the PDF numbers.
[b] Supports calcined at 970 K. These values did not change after the incorporation of cobalt.
[c] XRD patterns did not show any $La_2Zr_2O_7$ peak.

TABLE 5

Hydrogen Consumption Measured during TPR Experiments[a]

Catalyst	H_2^b/Co	Reduction peak at 420–470 K, $(H_2/Co)_{low}$
$Co(0.42)ZrO_2$	1.4	0.29
$Co(0.95)ZrO_2$	1.3	0.07
$Co(1.9)ZrO_2$	1.2	0.14
$Co(1.9)/ZrO_2$	1.0	0.09
$Co(0.38)La/ZrO_2$[c]	0.9	0.08
$Co(0.90)La/ZrO_2$[c]	0.8	0.13
$Co(1.8)La/ZrO_2$[c]	0.8	0.08
$Co(3.3)/La_2O_3$[d]	1.5	No peak
$LaCoO_3$	1.3	No peak

[a] The heating rate was 10 K/min from 320 to 1170 K flowing 5 vol% of hydrogen in argon at 40 cm^3 min^{-1}.

[b] Total H_2 consumption.

[c] Bulk carbonates are present in La_2O_3/ZrO_2-supported oxides (estimated amount is 0.3 wt% ($La_2O_2CO_3$ + $La_2(CO_3)_3$)).

[d] For La_2O_3-supported oxides the estimated amount of bulk carbonates is 4 wt% ($La_2O_2CO_3 + La_2(CO_3)_3$).

no appreciable surface area changes were observed for all the catalysts.

In order to study the thermal stability of the solids, $Co(0.42)ZrO_2$ and $Co(0.38)La/ZrO_2$ were treated at 970 K for more than 150 h in steam-saturated air (3% H_2O). After this treatment there were no changes in BET areas.

TPR Experiments

They were performed to obtain indirect information about the presence of other compounds not detected through XRD. Table 5 shows the total hydrogen consumption between room temperature and 1170 K for cobalt supported on several solids. $LaCoO_3$ is included for comparison.

Taking into account the different cobalt oxidation states, the theoretical values of hydrogen consumption (considering 100% reduction of cobalt) are the following:

(i) Co^{2+}, $H_2/Co = 1$ and

(ii) Co^{3+}, $H_2/Co = 1.5$

For mixtures of both, the H_2/Co ratio will be somewhere between these two values. Note that in the presence of Co^{3+} one could observe the stepwise reductions of Co^{3+} to Co^{2+} followed by Co^{2+} to Co^o.

For $LaCoO_3$, the expected H_2/Co is 1.5 while the experimental value is 1.3. The difference could be attributed to the La_2O_3 segregation observed in this perovskite (16). The group of ZrO_2-containing catalysts exhibits cobalt species reducible at temperatures below 670 K, while in the case of La_2O_3-supported oxides, reduction peaks appear at higher temperatures. This indicates that zirconium-containing oxides have cobalt species that are easier to reduce than lanthanum-containing ones. Besides, at 1170 K all the TPR profiles of both cobalt- and cobalt–lanthanum-containing ZrO_2 show the beginnings of a high-temperature reduction peak. This, as well as the values given in Table 5, indicates the presence of cobalt species that are not reduced up to 1170 K. These species should correspond to strong cobalt–zirconia and cobalt–lanthanum–zirconia interactions.

Note that the cobalt supported on ZrO_2 and La_2O_3/ZrO_2 catalysts exhibits a reduction peak at 420–470 K that appears neither in cobalt supported on La_2O_3 nor in the perovskite. Moreover, this peak is absent in the supports ZrO_2, La_2O_3/ZrO_2, or La_2O_3. The hydrogen consumption is ca. $H_2/Co = 0.1$ in all these cases, except for $Co(0.42)ZrO_2$. In order to confirm that these peaks are real reduction peaks, TPR profiles were run using reduced samples and they did not appear.

All the lanthanum-containing samples have bulk carbonates in varying proportions. In order to eliminate them before running the TPR experiments, all the solids were pretreated with H_2 (5 vol%)/Ar at 920 K for 30 min and then reoxidized with oxygen at 820 K for another 30 min. Afterward, the TPR was done using 5% of hydrogen in argon, 40 $cm^3 \cdot min^{-1}$, with a heating rate of 10 K min^{-1}, from 320 to 1170 K. The amount of carbonates was calculated from the difference between hydrogen consumption before and after this treatment. It was assumed that the carbonates and oxycarbonates were present in equimolar proportions:

$$La_2(CO_3)_3 + 12H_2 \Leftrightarrow 3CH_4 + La_2O_3 + 6H_2O$$

$$La_2(CO_3)_3 + 4H_2 \Leftrightarrow CH_4 + La_2O_3 + 2H_2O.$$

The results obtained are shown in footnotes *c* and *d* of Table 5.

XPS Data

Figure 3 shows the Co 2*p* photoelectron spectra obtained for the different supported oxides under study. Note the presence of Co^{2+} revealed by the shake-up peak of the Co $2p_{3/2}$ signal in all the solids studied, except on $Co(3.3)/La_2O_3$ and $LaCoO_3$. At higher binding energy values, there appear the Co $2p_{1/2}$ signals and the corresponding shake-up peaks (when Co^{2+} is present). $Co(0.42)ZrO_2$ and $Co(0.38)La/ZrO_2$ are not shown in this figure but they also exhibit the presence of surface Co^{2+}. In the case of $Co(0.27)La_2O_3$, surface cobalt could not be detected, due to the small amount of transition metals contained in this oxide.

Table 6 summarizes the XPS data obtained for all the solids. The second column shows the Co $2p_{3/2}$ B.Es., taking the C 1*s* (284.9 eV) as reference. Note the higher values observed in the $Co(n)ZrO_2$ compared with those of $Co(n)La/ZrO_2$. However, all these values are larger that those reported in the literature for Co $2p_{3/2}$ in oxides (10, 20, 21). This might be due to the broad C 1*s* signals recorded in all these samples (2.8 eV), which impairs the peak deconvolution. Trying to overcome this difficulty, the lattice O 1*s* signal was taken as reference to calculate the values shown

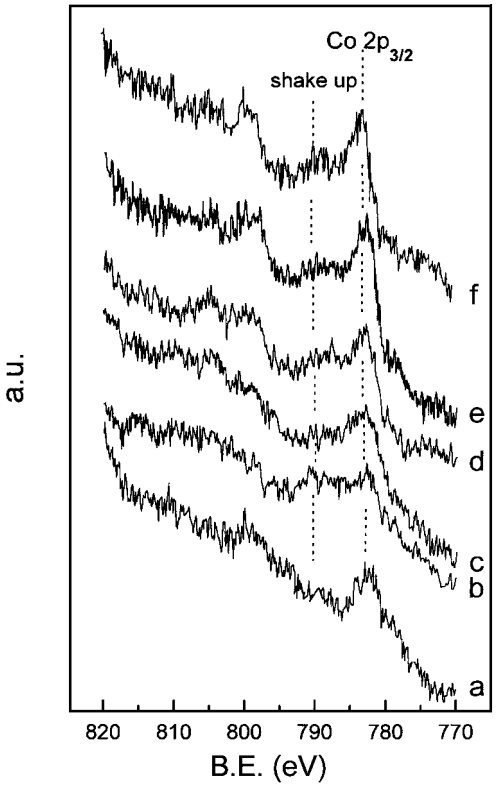

FIG. 3. Co 2*p* core level spectra of (a) Co(3.3)/La_2O_3, (b) Co(0.90)La/ZrO_2, (c) Co(1.8)La/ZrO_2, (d) Co(0.95)ZrO_2, (e) Co(1.9)ZrO_2, and (f) Co(1.9)/ZrO_2. The Co $2p_{3/2}$ peak and the corresponding shake-up satellite are indicated.

in column 3. In this way, all the B.Es. of Co $2p_{3/2}$ were decreased although a difference between catalysts with and without lanthanum still exists.

The surface Co/(La + Zr) ratio (column 5) increases as expected with the number of ALE reaction cycles for cobalt supported on both ZrO_2 and La_2O_3/ZrO_2. Note that the increase is higher from the first to the third cycle than from the latter to the fifth. The same tendency is observed for the reaction rates at 770 K (Fig. 4).

Note that the aged catalysts behave in a different way. In the case of Co(1.8)La/ZrO_2-aged, the atomic surface Co/(La + Zr) ratio is practically the same as that of the fresh catalyst, but in the case of Co(1.9)ZrO_2, the Co $2p_{3/2}$ signal is too noisy so that the Co/Zr atomic surface ratio could not be calculated (Table 6).

The Kerkhof–Moulijn model (22), simplified by V. León (23), allowed us to obtain qualitative and quantitative results from XPS atomic concentrations using accepted approximations on the corresponding electron mean free paths for supported fresh catalysts. The pertinent equation obtained from the model applied to cobalt supported on ZrO_2 can be written as

$$(\mathrm{Co/Zr})_{\mathrm{Surf}} = (\mathrm{Co/Zr})_{\mathrm{Bulk}} BC \qquad [6]$$

$$B = (0.5\beta)[(1 + e^{-\beta})(1 - e^{-\beta})^{-1}]; \qquad \beta = 2(\delta S \lambda_{\mathrm{CoZr}})^{-1}$$

$$C = (1 - e^{-\alpha})\alpha^{-1}; \quad \alpha = c(\lambda_{\mathrm{CoCo}})^{-1},$$

TABLE 6

Surface Characteristics of the Supported Oxides

Catalysts	Co $2p_{3/2}$[a] B. E. (eV)	Co $2p_{3/2}$[b] B. E. (eV)	Presence of Co^{2+}	Co/(La + Zr)
Co(0.42)ZrO_2	782.6	781.2	Yes[c]	0.07
Co(0.95)ZrO_2	782.6	781.6	Yes[c]	0.12
Co(1.9)ZrO_2	782.7	781.1	Yes[c]	0.14
Co(1.9)ZrO_2-aged[d]	—[e]	—[e]	—[e]	—[e]
Co(1.9)/ZrO_2	782.7	781.0	Yes[c]	0.13
Co(0.38)La/ZrO_2	782.6	781.0	Yes[c]	0.07
Co(0.90)La/ZrO_2	781.4	780.8	Yes[c]	0.12
Co(1.8)La/ZrO_2	781.7	780.8	Yes[c]	0.15
Co(1.8)La/ZrO_2-aged[d]	781.6	781.0	Yes[c]	0.13
Co(3.3)/La_2O_3	780.4	780.8	No	0.25
$LaCoO_3$[f]	779.7	—	No	0.7

[a] Binding energies corrected using the value of 284.9 eV for the C 1*s* peak (contamination carbon).

[b] Binding energies corrected using the value of 530.0 eV for the O 1*s* peak (lattice oxygen).

[c] The spectra exhibited the presence of Co^{2+} ions (indicated by the appearance of the satellite peak, characteristic of Co^{2+} in a high-spin state).

[d] Aging treatment consisted of 150 h on stream at 970 K.

[e] Very weak noisy cobalt signal that could not be quantified.

[f] The perovskite was prepared by the explosion method (16) and it was analyzed using a monochromatic XPS instrument (7).

where

—$(\mathrm{Co/Zr})_{\mathrm{Surf}}$ is the ratio of XPS atomic concentration of cobalt and the support cation.

—$(\mathrm{Co/Zr})_{\mathrm{Bulk}}$ is the bulk Co/Zr atomic ratio.

—β depends on the support real density (δ) and its accessible surface area (S) and on λ_{CoZr}, which is the cobalt electron mean free path through the support phase. λ_{CoZr} is approximated to λ_{ZrZr}, so that the B parameter depends only on the support.

—C depends only on the average "crystal" size of the supported cobalt phase (c) and λ_{CoCo}, the mean free path

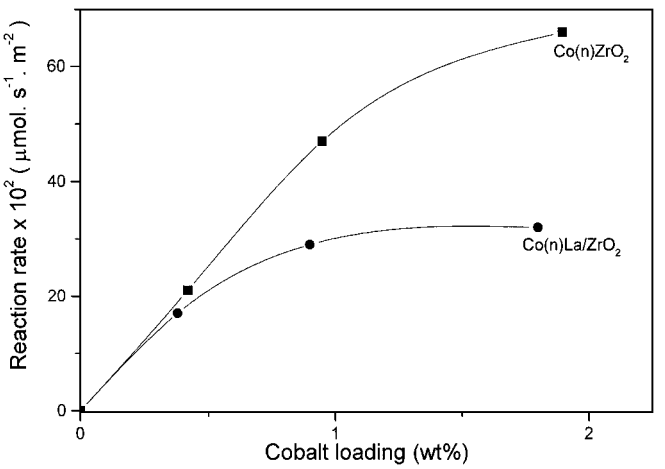

FIG. 4. Effect of the cobalt loading upon the reaction rates for methane combustion at 770 K (good catalysts).

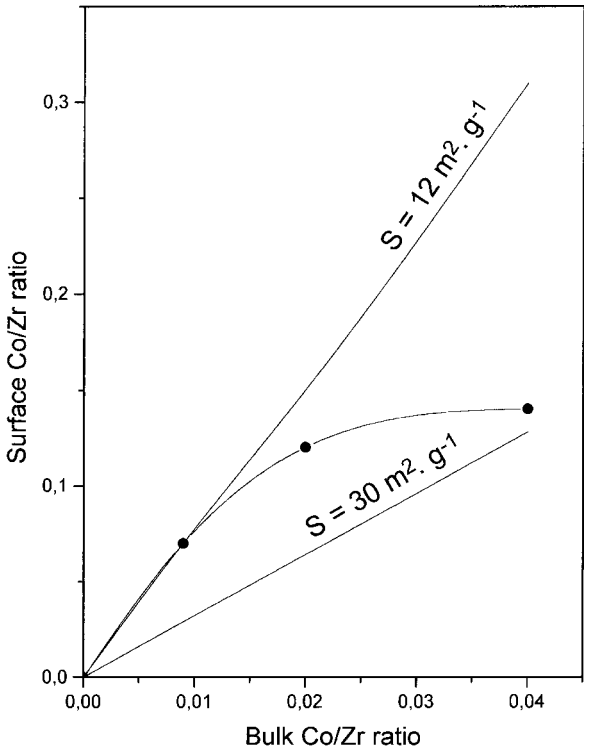

FIG. 5. Increase in surface Co/Zr ratio with cobalt loading ($Co(n)ZrO_2$, ALE method) (●). Two straight lines calculated using a simplified Kerkhof–Moulijn model (22) are included: (i) considering the surface area of the support ($30\ m^2 \cdot g^{-1}$) and (ii) taking into account the accessible area of $12\ m^2 \cdot g^{-1}$ (see text).

of cobalt electrons passing through the supported cobalt; therefore, the C parameter depends only on the supported oxide.

$(Co/Zr)_{Surf}$ varies linearly with $(Co/Zr)_{Bulk}$ with a slope B for monoatomic patch coverage because $C = 1$. In the case of polyatomic patches, $0 < C < 1$.

Figure 5 shows the experimental $(Co/Zr)_{Surf}$ ratio as a function of cobalt bulk concentration. Considering the nature of the ALE process, the first ALE reaction cycle only produces monoatomic islands, so that the calculation of the B parameter leads to an estimation of the accessible surface, $S = 12\ m^2 \cdot g^{-1}$, which corresponds to 40% of the total surface area. This suggests that cobalt is mostly deposited on the external surface of ZrO_2 grains during the first cycle. The lower straight line corresponds to the total surface area ($30\ m^2 \cdot g^{-1}$). The convexity in the experimental curve could be due either to the formation of polyatomic islands ($C < 1$), or to the increase in surface coverage, in which case B decreases, or both. Since the rate data (Fig. 4) show a plateau similar to the experimental curve, it is concluded that the formation of multilayers is responsible for this behavior.

DISCUSSION

Table 7 summarizes the main features that differentiate the good from the bad catalysts for methane combustion. The appearance of a low-temperature peak in the TPR profiles of good catalysts may be connected to the presence of Co^{2+} on the surface of these solids (Table 7). The low-temperature H_2 consumed could be used to reduce O_2 chemisorbed on Co^{2+} centers. It is unlikely, on the other hand, that Co^{2+} might be connected to the presence of Co_3O_4 on the catalyst surface. This is supported by the absence of the main reflections of Co_3O_4 in the XRD patterns of the ALE prepared catalysts containing ca. 2 wt% Co. Moreover, when the Co_3O_4 reflections are detected in $Co(3.3)/La_2O_3$ no Co^{2+} is seen on the surface (Fig. 3, spectrum a). We propose that these surface Co^{2+} species are associated with CoO_x moieties lying on the top of the polyatomic islands.

TABLE 7

Catalytic Activity and Main Features of Co-Containing Catalysts

Features	Activity: Good; Rate = 0.2–0.7 $\mu mol \cdot s^{-1} \cdot m^{-2}$	Activity: Bad; Rate < 0.05 $\mu mol \cdot s^{-1} \cdot m^{-2}$
$(H_2/Co)_{low}$ (TPR)	Ca. 0.1	None
Co^{2+} (XPS)	Present	Absent
Bulk carbonates (TPR[a] and XRD)	Small amounts	Significant amounts
Surface carbonates (XPS)	Small signals	Large signals

[a] See footnotes *c* and *d* of Table 5.

At first sight, the large decrease in the reaction rates of Co supported on La_2O_3/ZrO_2, $Co(3.3)/La_2O_3$, and $LaCoO_3$ (Table 3) are surprising since the surface Co content increases in the opposite direction (Table 6). Table 7 shows that the bad catalysts such as the latter two exhibit significant amounts of bulk and surface carbonated species. At this point, it should be recalled that La_2O_3 reacts with CO_2 to form carbonated species (7). In fact, going back to Table 3, it is clearly seen that $Co(3.3)/La_2O_3$, $LaCoO_3$, $Co(0.27)La_2O_3$, and pure La_2O_3 have essentially the same catalytic activity due to the presence of surface carbonated species, as discussed in more detail elsewhere (7).

Now it is convenient to discuss cobalt supported on ZrO_2 and then to consider the incorporation of lanthanum in to this system. From data given in Table 2 it is clear that an increase in the number of the cobalt ALE reaction cycles results in increasing total cobalt contents, but this is not completely reflected by the Co/Zr atomic ratio on the outlayers of the catalyst (Table 6). Using a simplified Kerkhof–Moulijn model for dispersion quantification from XPS atomic concentrations (22, 23), it was concluded that beyond the first cycle mostly polyatomic islands are formed on the ZrO_2 surface (Fig. 5).

The TPR results are symptomatic of a strong Co–Zr interaction. The hydrogen consumption per cobalt atom decreases as the Co content in the solid increases, indicating

either the formation of cobalt species that are more difficult to reduce (Table 5), or the increase in Co^{2+} concentration. The former hypothesis is further supported by the high-temperature curvature of the TPR profiles, indicating incomplete reduction of the solids up to 1170 K.

The cobalt-impregnated ZrO_2 catalyst ($Co(1.9)/ZrO_2$) deserves special analysis. To begin with, it is several times less active than the ALE-prepared $Co(1.9)ZrO_2$ (Table 3). However, both catalysts contain the same cobalt loading and the same surface Co/Zr ratio (Table 6). The TPR data (Table 5) seem to offer a clue to explain the difference in activity. Note that the total hydrogen consumed is lower for the impregnated catalyst, indicating a stronger interaction between the transition metal and the support with the formation of Co–Zr species. To complete the explanation, the contribution of Co–Zr species to the activity for methane combustion would not be comparable with that of CoO_x moieties lying on top of polyatomic islands. These sites would be responsible for the high activity shown by $Co(1.9)ZrO_2$ obtained using the ALE technique.

Let us go back to cobalt supported on La_2O_3/ZrO_2. Values of surface Co/(La+Zr) are similar to those obtained for cobalt supported on ZrO_2 (Table 6) although reaction rates (Table 3) and reduction levels (Table 5) are lower. This suggests a different interaction between Co and lanthanum-doped ZrO_2. In this regard, Table 6 shows consistently lower Co $2p_{3/2}$ B.Es. in the catalysts containing La than those recorded in the $Co(n)ZrO_2$ solids.

Mizuno et al. (10) prepared $LaCoO_3$ highly dispersed on ZrO_2 and found that the reaction between La–Co oxide and ZrO_2 to form $La_2Zr_2O_7$ and Co_3O_4 occurred at loadings higher than 7.5 wt% (Co + La) or during calcination above 1120 K. According to this result, cobalt was expected to exist as Co_3O_4 and/or $LaCoO_3$ in our samples. So, the hydrogen consumption values should be somewhere between 1.3 and 1.5 H_2/Co. This range is approached only in certain cases such as $Co(3.3)/La_2O_3$ and bulk $LaCoO_3$, but this is not the case with the three $Co(n)La/ZrO_2$ solids.

Besides, although $Co(1.8)La/ZrO_2$, $Co(1.9)ZrO_2$, and $Co(1.9)/ZrO_2$ have practically the same cobalt content and similar surface concentrations, the Co $2p_{3/2}$ signal appears at a lower B.E. value in the case of the lanthanum-containing catalyst (Table 6). This observation together with the TPR data (Table 5) are symptomatic of a cobalt–support interaction of a different nature probably involving La, Co, and Zr.

The estimation of the percentage of the effective area using the simplified Kerkhof–Moulijn model for La_2O_3/ZrO_2-supported catalysts is difficult because the presence of La_2O_3 on ZrO_2 grains complicates the estimation of the β parameter of Eq. [6]. However, the tendency of the Co/(Zr + La) atomic surface ratio as a function of the total cobalt content (Table 6) is the same as that found for $Co(n)ZrO_2$. This could mean that the "apparent saturation" of the surface Co/(La + Zr) ratio (Fig. 4) is also due to the formation of three-dimensional patches.

Catalyst Stability

According to the rate data (Table 3), the addition of lanthanum decreases the activity of $Co(n)ZrO_2$ catalysts. Nevertheless, as already said in the catalytic results section, preliminary long-term experiments (>150 h on stream at 970 K) seem to indicate that La_2O_3/ZrO_2-supported solids are more stable catalysts than those not containing lanthanum oxide.

Which Is the Role of Lanthanum in $Co(n)La/ZrO_2$ Formulations?

—The surface area of the aged catalysts could not be measured due to the small amount of solid used in the reactor to minimize thermal effects. However, the constancy of the surface area verified after treating cobalt zirconia and cobalt–lanthanum zirconia at 970 K for 150 h in flowing wet air seems to indicate that surface area instability does not play a role in the deactivation of these catalysts.

—X-ray diffraction patterns were not altered in the aged catalysts.

—The surface properties of $Co(1.9)ZrO_2$ are modified after 150 h on stream. The atomic Co/(La + Zr) surface ratio obtained for $Co(1.8)La/ZrO_2$-aged is 0.13 (similar to that obtained for the fresh catalyst). Nevertheless, for $Co(1.9)ZrO_2$ the small and noisy Co $2p_{3/2}$ signal indicates a significant decrease in the surface cobalt concentration for the aged catalyst. Thus, the stability of La_2O_3/ZrO_2-supported catalysts could be related to the retention of the transition metal on the catalyst surface.

Undoubtedly, more work is needed in order to better understand the nature of the increased stability of the $Co(n)La/ZrO_2$ solids.

CONCLUSIONS

Cobalt supported on ZrO_2 or La_2O_3/ZrO_2 is 1 order of magnitude more active than Co/La_2O_3 or the perovskite $LaCoO_3$ for the total combustion of methane at high temperatures.

Conditions being identical, the catalyst prepared using the atomic layer epitaxy technique is several times more active than the one obtained using the classical wet impregnation approach (Table 3, rows 3 and 4).

The presence of a low-temperature (420–470 K) reduction peak, Co^{2+} on the surface and the absence of highly stable carbonates are the common features of the best catalysts (Table 7).

Lanthanum carbonates and oxycarbonates are very stable at temperatures up to 1220 K (7). The low-activity catalysts including La_2O_3 contain bulk carbonates and show

intense C 1*s* carbonate signals. The surface carbonate layer masks the catalytic action of the transition metal.

The presence of lanthanum on ZrO_2 seems to slow cobalt migration inside the zirconia lattice, sharply decreasing the rate of deactivation of these solids compared to that of pure ZrO_2. This point deserves additional research to better understand the deactivation processes in the catalysts.

ACKNOWLEDGMENTS

The authors acknowledge the financial support received from CONICET, UNL (CAI + D '96), and ANPCyT. Thanks are also given to the Japan International Cooperation Agency (JICA) for the donation of the XPS, TPR, and XRD instruments and to Elsa Grimaldi for the English edition of the manuscript.

REFERENCES

1. Zwinkels, M., Järås, S., and Menon, P., *Catal. Rev.-Sci. Eng.* **35**, 319 (1993).
2. McCarty, J., Gusman, M., Lowe, D., Hildenbrand, D., and Lau, K., *Catal. Today* **47**, 5 (1999).
3. XONON Systems, catalytica.inc.com, October 8, 1998.
4. Dalla Betta, R. A., *Catal. Today* **35**, 129 (1997).
5. McCarty, J., and Wise, H., *Catal. Today* **8**, 231 (1990).
6. Nitadori, T., Ichiki, T., and Misono, M., *Bull. Chem. Soc. Jpn.* **61**, 621 (1988).
7. Milt, V. G., Spretz, R., Ulla, M. A., and Lombardo, E. A., *Catal. Lett.* **42**, 57 (1996).
8. Ferri, D., and Forni, L., *Appl. Catal. B: Environmental* **16**, 119 (1998).
9. Connell, M., Norman, A., Hüttermann, C., and Morris, M., *Catal. Today* **47**, 123 (1999).
10. Mizuno, N., Fujii, H., Igarashi, H., and Misono, M., *J. Am. Chem. Soc.* **114**, 7151 (1992).
11. Kytökivi, A., Jacobs, J., Hakuli, A., Merilainen, J., and Brongersma, H., *J. Catal.* **162**, 190 (1996).
12. Jacobs, J., Lindfors, L., Reintjes, J., Jylha, O., and Brongersma, H., *Catal. Lett.* **25**, 315 (1994).
13. Lindblad, M., Lindfors, L., and Suntola, T., *Catal. Lett.* **27**, 323 (1994).
14. Suntola, T., *Appl. Surf. Sci.* **100/101**, 391 (1996).
15. Haukka, S., Lakomaa, E., and Suntola, T., *Appl. Surf. Sci.* **75**, 220 (1994).
16. Milt, V. G., Spretz, R., Ulla, M. A., and Lombardo, E. A., *J. Mater. Sci. Lett.* **14**, 428 (1995).
17. Carberry, J. J., "Chemical and Catalytic Reaction Engineering." McGraw-Hill, New York, 1976.
18. Heck, R. M., and Farrauto, R. J., "Catalytic Air Pollution Control, Commercial Technology." Van Nostrand Reinhold, New York, 1995.
19. Milt, V. G., Ulla, M. A., and Lombardo, E.A., *Catal. Lett.* **65**, 67 (2000).
20. Payen, L., Gengembre, L., Mauge, F., Duchet, J. C., and Lavalley, J. C., *Catal. Today* **10**, 521 (1991).
21. Nudel, J. N., Umansky, B. S., and Lombardo, E. A., *Appl. Catal.* **26**, 339 (1986).
22. Kerkhof, F. P. J. M., and Moulijn, J. A., *J. Phys. Chem.* **83**, 1612 (1979).
23. León, V., *Surf. Sci.* **339**, L931 (1995).